

# On the convective instability of hot radiative accretion flows

Feng Yuan<sup>1\*</sup> and De-Fu Bu<sup>1,2†</sup>

<sup>1</sup>*Key Laboratory for Research in Galaxies and Cosmology, Shanghai Astronomical Observatory, Chinese Academy of Sciences, 80 Nandan Road, Shanghai 200030, China*

<sup>2</sup>*Graduate School of the Chinese Academy of Sciences, Beijing 100039, China*

29 May 2018

## ABSTRACT

How many fraction of gas available at the outer boundary can finally fall onto the black hole is an important question. It determines the observational appearance of accretion flows, and is also related with the evolution of black hole mass and spin. Previous two-dimensional hydrodynamical simulations of hot accretion flows find that the flow is convectively unstable because of its inward increase of entropy. As a result, the mass accretion rate decreases inward, i.e., only a small fraction of accretion gas can fall onto the black hole, while the rest circulates in the convective eddies or lost in convective outflows. Radiation is usually neglected in these simulations. In many cases, however, radiative cooling is important. In the regime of the luminous hot accretion flow (LHAF), radiative cooling is even stronger than the viscous dissipation. In the one dimensional case, this implies that the inward increase of entropy will become slower or the entropy even decreases inward in the case of an LHAF. We therefore expect that convective instability becomes weaker or completely disappears when radiative cooling is important. To examine the validity of this expectation, in this paper we perform two-dimensional hydrodynamical simulations of hot accretion flows with strong radiative cooling. We find that compared to the case of negligible radiation, convection only becomes slightly weaker. Even an LHAF is still strongly convectively unstable, its radial profile of accretion rate correspondingly changes little. We find the reason is that the entropy still increases inward in the two-dimensional case.

**Key words:** accretion, accretion discs – hydrodynamics: HD – ISM: jets and outflow – black hole physics

## 1 INTRODUCTION

Hot accretion flows such as advection-dominated accretion flows (ADAFs) are interesting because they are likely operating in low-luminosity active galactic nuclei (AGNs) and hard and quiescent states of black hole X-ray binaries (see Narayan 2005; Yuan 2007; Narayan & McClintock 2008 for recent reviews). ADAFs are originally proposed and studied by vertically-integrated one-dimensional method since the global two-dimensional solution is technically too difficult to obtain (e.g., Narayan & Yi 1994; 1995; Abramowicz et al. 1995). While this approach has discovered the main properties of ADAFs, some important multi-dimensional effects such as convection and outflow as we will focus in this pa-

per are neglected and await the multi-dimensional numerical simulations.

Perhaps the most important finding of multi-dimensional hydrodynamical simulations is that the flows are highly convectively unstable (Igumenshchev & Abramowicz 1999, hereafter IA99; Stone, Pringle & Begelman 1999, hereafter SPB99; Igumenshchev & Abramowicz 2000), in consistent with what suggested by one-dimensional self-similar solution of ADAFs (Narayan & Yi 1994; 1995). The physical reason is that the entropy of the accretion flow increases inward. Because of the convective instability, most of the gas available at the outer boundary can't fall onto the horizon of the central black hole, but circulates in convective eddies or lost in convective outflows. As a result, the mass accretion rate keeps decreasing inward.

The radial profile of accretion rate has important observational implications. The radiative appearance of black hole obviously depends on it. This is crucial for us to explain

\* E-mail: fyuan@shao.ac.cn

† E-mail: dfbu@shao.ac.cn

some observations. The first example is the supermassive black hole in the Galactic center, Sgr A\*. *Chandra* observations combined with Bondi accretion theory present a robust estimation to the value of accretion rate at the outer boundary of the accretion flow, the Bondi radius, which is about  $10^{-5} M_{\odot} \text{ yr}^{-1}$  (Baganoff et al. 2003). On the other hand, the detected high linear polarization at radio waveband requires a mass inflow rate of only  $10^{-7}$ - $10^{-9} M_{\odot} \text{ yr}^{-1}$  at the innermost region of the ADAF (Marrone et al. 2007). So most of the gas can't fall onto the black hole. The second example is the transition from hard to soft states of black hole X-ray binaries. The model of the hard state is an inner hot accretion flow plus an outer truncated thin disk outside of the truncation radius  $R_{\text{tr}}$ , while the soft state is described by a standard thin disk. One well-known observational result is that the luminosity changes little during the transition (e.g., Zdziarski et al. 2004). This requires that the accretion rate of the inner hot accretion flow should not decrease significantly inward from  $R_{\text{tr}}$ , because otherwise we would expect that the luminosity had increased significantly after the transition due to the higher accretion rate of the thin disk. In addition to the effects on the emitted spectrum, the exact profile of accretion rate is also important to the study of evolution of black hole mass and spin at least in the phase of low-luminosity AGNs (LLAGNs), in which a hot accretion flow is believed to be working (Ho 2008).

In all numerical simulations mentioned above, however, radiation is neglected. This is a good approximation only when the mass accretion rate is very low so radiative cooling is unimportant. In reality, the accretion rate is often high enough thus radiative cooling can't be neglected. Moreover, when the accretion rate is high enough, such as in the luminous hard state and LLAGNs, the flow will enter into the regime of luminous hot accretion flow (LHAF; Yuan 2001; 2003). In this case, the radiative cooling rate is higher than the viscous dissipation rate. In one-dimensional case, this implies that the entropy of the gas *decreases* inwardly (see Yuan 2001 or §3.2 in this paper for details). Therefore, different from an ADAF, an LHAF is predicted to be convectively stable (Yuan 2001).

In the present work, we simulate the two-dimensional hydrodynamical accretion flow with radiation. We do this by adding bremsstrahlung radiation in the energy equation. Our purpose is to examine the effects of radiation on the dynamics of hot accretion flow, especially on the convective instability. Surprisingly, our results indicate that the accretion flow is still convectively unstable, even when the flow is in the regime of an LHAF. In Section 2, we describe our numerical method. Results are described in Section 3. We summarize and discuss our results in Section 4.

## 2 METHOD

### 2.1 The equations of motion

The hydrodynamical equations describing accretion including bremsstrahlung radiation are:

$$\frac{d\rho}{dt} + \rho \nabla \cdot \mathbf{v} = 0, \quad (1)$$

$$\rho \frac{d\mathbf{v}}{dt} = -\nabla p - \rho \nabla \psi + \nabla \cdot \mathbf{T}, \quad (2)$$

$$\rho \frac{d(e/\rho)}{dt} = -p \nabla \cdot \mathbf{v} + \mathbf{T}^2/\mu - Q_{\text{rad}}^-, \quad (3)$$

where  $\rho$ ,  $p$ ,  $\psi$ ,  $\mathbf{v}$ ,  $e$  and  $\mathbf{T}$  are density, pressure, gravitational potential, velocity, internal energy and anomalous stress tensor, respectively. The  $d/dt (\equiv \partial/\partial t + \mathbf{v} \cdot \nabla)$  denotes the Lagrangian time derivative. We adopt an equation of state of ideal gas  $p = (\gamma - 1)e$ , and consider models with  $\gamma = 5/3$ . We assume bremsstrahlung cooling  $Q_{\text{rad}}^- = 6.2 \times 10^{20} \rho^2 T^{1/2} \text{ erg} \cdot \text{s}^{-1} \cdot \text{cm}^{-3}$ , with  $T$  is the temperature of the accretion flow.

We use the stress tensor  $\mathbf{T}$  to mimic the shear stress which is in reality magnetic stress associated with MHD turbulence driven by the magneto-rotational instability (MRI; Balbus & Hawley 1998). Following SPB99, in most cases, we assume that the only non-zero components of  $\mathbf{T}$  are the azimuthal ones:

$$T_{r\phi} = \mu r \frac{\partial}{\partial r} \left( \frac{v_{\phi}}{r} \right), \quad (4)$$

$$T_{\theta\phi} = \frac{\mu \sin \theta}{r} \frac{\partial}{\partial \theta} \left( \frac{v_{\phi}}{\sin \theta} \right). \quad (5)$$

This is because the MRI is driven only by the shear associated with orbital dynamics. But in order to compare with previous works we also use the full components in the case of large  $\alpha$  (§3.3). Following SPB99, in most calculations we adopt the coefficient of shear viscosity  $\mu = \nu \rho$  and the magnitude of the kinematic coefficient  $\nu = 0.1 \rho / \rho_{\text{max}}$ . Here  $\rho_{\text{max}}$  is the maximum density of the initial torus adopted in our simulation (see §2.2 below).

We use pseudo-Newtonian potential to mimic the general relativistic effects,  $\psi = -GM/(r - r_s)$ , where  $G$  is the gravitational constant,  $M$  is the mass of the black hole, and  $r_s = 2GM/c^2$  is the Schwarzschild radius. We neglect the self-gravity of the disk.

### 2.2 Initial conditions

Following SPB99, the initial state of our simulations is an equilibrium torus with constant specific angular momentum. The equilibrium structure of the torus is given by (Papaloizou & Pringle 1984)

$$\frac{p}{\rho} = \frac{(\gamma - 1)GM}{\gamma R_0} \left[ \frac{R_0}{r} - \frac{1}{2} \left( \frac{R_0}{r \sin \theta} \right)^2 - \frac{1}{2d} \right]. \quad (6)$$

Here  $R_0$  is the radius of the center (density maximum) of the torus, and  $d$  is the distortion of the torus. As used in SPB99, our torus is embedded in a low density medium. The density and the pressure of the medium are  $\rho_m$  and  $p_m = \rho_m/r$ , respectively.

The units adopted in our calculations are listed in table 1. Note that we introduce a parameter  $n$  in the unit of density. By setting it to be different values, we can adjust the density of the initial torus and thus the accretion rate. In this paper, we calculate three values of  $n$ , namely 1.2, 0.012 and 0.00012. They correspond to Model A, B, and C, respectively.

The radius of the maximum density is set as  $R_0 = 90r_s$ , the specific angular momentum of the initial torus equals to the Keplerian angular momentum at  $R_0$ , the maximum density of the torus  $\rho_{\text{max}} = 0.29$  and the density of the medium  $\rho_m = 10^{-4}$ .

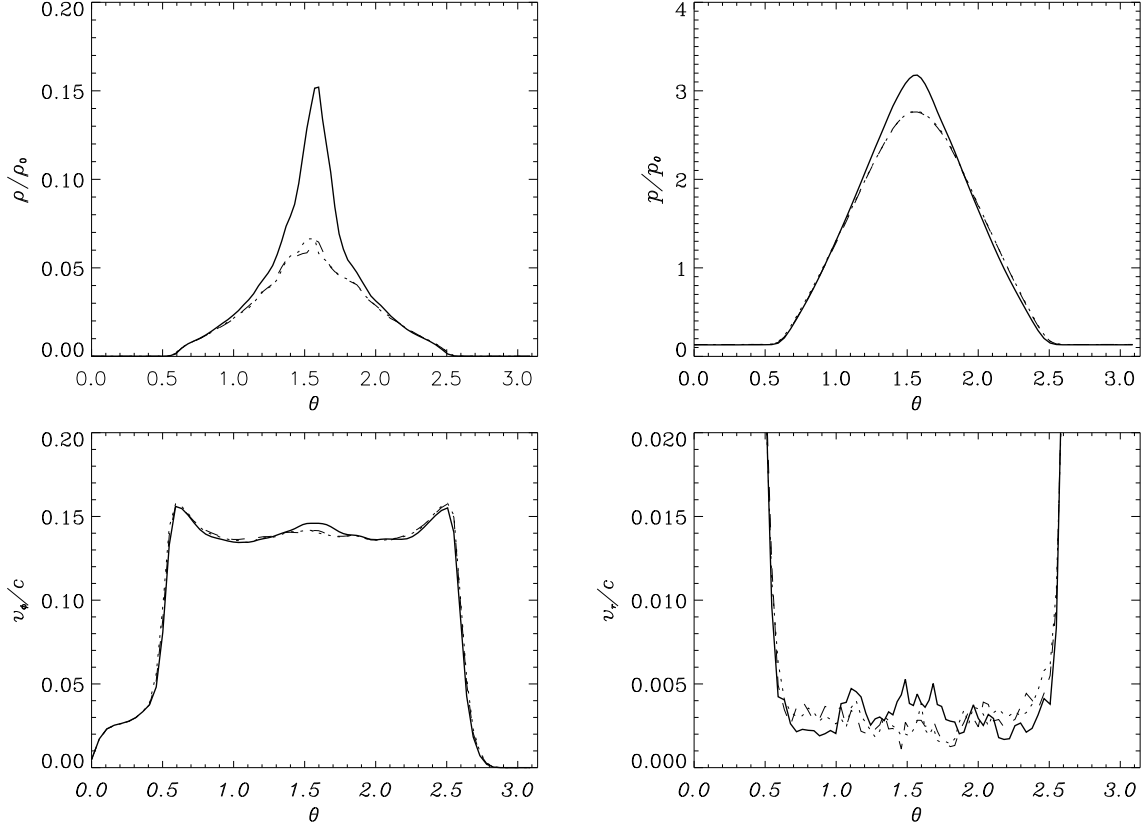


**Figure 1.** Angular profiles of a variety of time-averaged variables at  $r = 20r_s$ . The solid, dotted and dashed lines correspond to Model A, B, and C, respectively.

**Table 1.** Units adopted in the calculation

Physical quantity	Symbol	Numerical unit
Length	$r_g$	$3 \times 10^6 (M/10M_\odot) \text{ cm}$
Velocity	$c$	$2.9979 \times 10^{10} \text{ cm} \cdot \text{s}^{-1}$
Time	$t_0$	$5 \times 10^{-5} (M/10M_\odot) \text{ sec}$
Density	$\rho_0$	$2 \times 10^{-7} n(M/10M_\odot)^{-1} \text{ g} \cdot \text{cm}^{-3}$
Temperature	$T_0$	$1.1 \times 10^{13} \text{ K}$
Luminosity	$L_{Edd}$	$1.25 \times 10^{39} (M/10M_\odot) \text{ erg} \cdot \text{s}^{-1}$

### 2.3 Numerical methods

We use ZEUS-MP code (Hayes et al. 2006) in spherical geometry to solve the above equations. As a test, we have successfully reproduced all the results of SPB99. For our calculations, we set our computation grid extending from an inner boundary at  $r = 1.2r_s$  to  $300r_s$ . McKinney & Gammie (2002) show that the inner boundary must be smaller than the sonic point of the accretion flow, which is  $\sim 1.5r_s$ , otherwise the location of the inner boundary would affect the simulation results. We have also tried larger spacial range and find that the range adopted above does not affect our results, especially when the effects of radiative cooling are concerned, which is our main focus

of the present work. The number of grids is  $(N_r, N_\theta) = (180, 100)$ . We adopt non-uniform grid in the radial direction  $(\Delta r)_{i+1}/(\Delta r)_i = 1.0183$ . Similarly, we adopt non-uniform angular zones with  $(\Delta \theta)_{j+1}/(\Delta \theta)_j = 0.9826$  for  $0 \leq \theta \leq \pi/2$  and  $(\Delta \theta)_{j+1}/(\Delta \theta)_j = 1.0177$  for  $\pi/2 \leq \theta \leq \pi$ . Outflow boundary conditions are adopted at both the inner and outer radial boundaries. In the angular direction, the boundary conditions are set by symmetry at the poles.

## 3 RESULTS

### 3.1 The radial and angular structure

In this paper, time is measured in unit of orbital time at  $r = 90r_s$ . We switched on the radiative cooling term after 13 orbital time when the disk becomes quasi-steady. When radiative cooling is included, we find that it is quicker for the accretion flow to reach a steady state. This is because when the radiation is included, the density becomes more concentrated toward the equatorial plane, as shown by Figure 1. Since the ratio of viscous stress and other forces is proportional to  $\rho/\rho_{\max}$ , this results in a quicker establishment of a steady state. The reason of the concentration of the accretion flow is that the temperature decreases after the radiation cooling is included thus the accretion flow condenses.

Figure 1 shows the angular structure of the time-

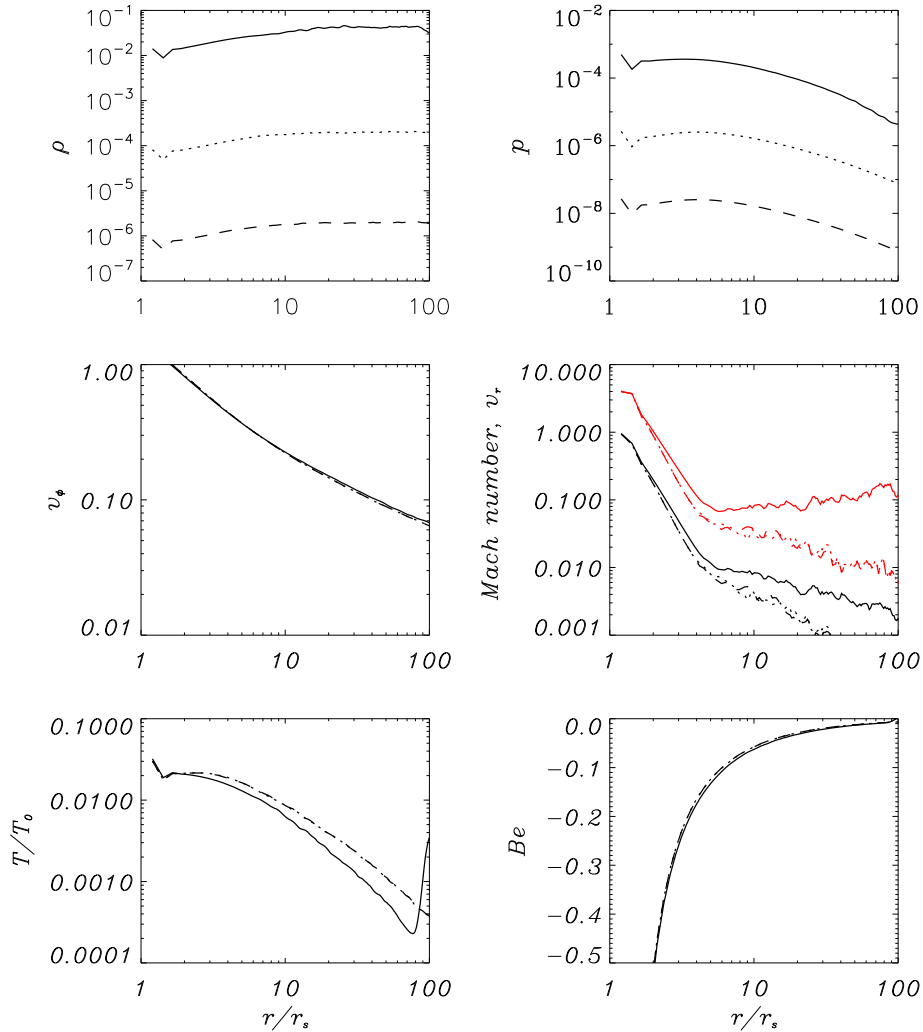


**Figure 2.** Radial scaling of some time-averaged quantities. The solution is averaged over angle between  $\theta = 84^\circ$  to  $\theta = 96^\circ$  and over 14 and 16 orbits. In every panel, the solid, dotted and dashed lines correspond to Model A, B, and C, respectively. The red and black lines in the middle-right panel correspond to the Mach number and radial velocity, respectively.

averaged variables at  $r = 20r_s$ . The solid, dotted and dashed lines correspond to Model A, B, and C, respectively. The density and gas pressure have been normalized in these figures. We can see from the figure that the dotted and dashed lines are almost superposed together, which implies that the radiative cooling is negligible in these two models. With increasing mass accretion rates, radiation becomes more and more important. As a result, the temperature decreases, so the density profile becomes more concentrated to the equatorial plane, i.e., the accretion flow becomes thinner. The concentration of density to the equatorial plane results in a larger radial velocity. But the effects of radiation on the angular velocities are very small. This is because the radiation pressure is negligible compared to the gas pressure.

Figure 2 shows the radial structure of the time-averaged flow near the equatorial plane. The solution is averaged over angle between  $\theta = 84^\circ$  to  $\theta = 96^\circ$ . In every panel, the solid, dotted and dashed lines correspond to Model A, B, and C, respectively. The red and black lines in the middle-right panel represent the Mach number and the radial velocity,

respectively. In all of our models the flows have become supersonic before they reach the inner boundary. This ensures that the location of inner boundary does not affect our results (McKinney & Gammie 2002). The density, gas pressure, rotation velocity and temperature in each model can be described by a radial power law, with  $\rho \propto r^0$ ,  $p \propto r^{-1}$ ,  $v_\phi \propto r^{-1/2}$  and  $T \propto r^{-1}$ . Especially, the Bernoulli parameter  $Be$  ( $Be \equiv v^2/2 + \gamma P/(\gamma - 1)\rho - GM/(r - r_s)$ ) for the three models are all below zero. The negative  $Be$  is different from the one-dimensional or two-dimensional self-similar results (Narayan & Yi 1994, 1995; see also Blandford & Begelman 1999) where the Bernoulli parameter along the equatorial plane is always positive when radiative cooling is weak. In our calculations, we set the kinetic viscosity coefficient  $\nu \propto \rho$  which is different from the usual “ $\alpha$ ” description adopted in previous works (Narayan & Yi 1994; 1995) which corresponds to  $\nu \propto r^{1/2}$ . But the discrepancy of the value of  $Be$  is not because of the difference of the viscosity description. SPB99 show that the value of  $Be$  is even more negative when  $\nu \propto r^{1/2}$ . The discrepancy is because when the accre-

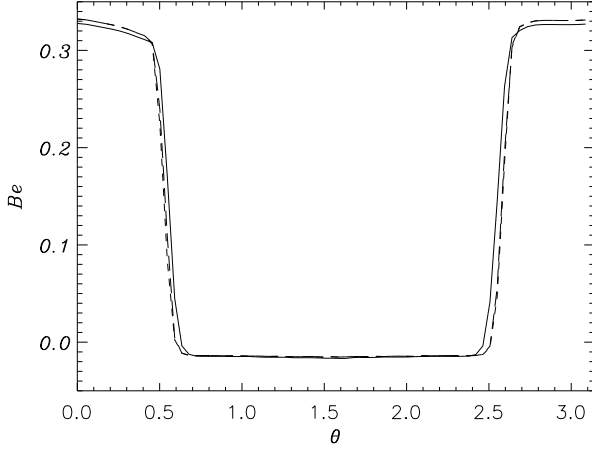


**Figure 3.** The distribution of Bernoulli parameter along the theta direction at  $40 r_s$ . The solid, dotted, and dashed lines correspond to Model A, B, and C, respectively.

tion flow is convectively unstable, the scaling law adopted in the above self-similar solution does not apply any more (Narayan, Igumenshchev & Abramowicz 2000; Quataert & Gruzinov 2000).

The negative nature of  $Be$  along the equatorial plane implies that very few of the accretion flow will escape and flow out to infinity (IA99; SPB99). To further investigate the strength of outflow, we show the angular structure of Bernoulli parameter  $Be$  at  $40 r_s$  in Figure 3. The angular profile of  $Be$  at other radii is similar to the profile at  $40 r_s$ . We can see that away from the equatorial plane, its value becomes larger, consistent with the prediction of Narayan & Yi (1995). It becomes positive close to the polar region. This is because the viscous stress transfer energy from the equator to the pole. Since the density in that region is very low, we can expect that the unbound outflow will be extremely weak. Our simulations show that the mass flux of unbound outflow is only  $\sim 1\%$  of the inflow flux. To produce strong unbound outflow, other mechanism such as large-scale magnetic field is required. Or, we should properly take into account the radiative transfer, as we will discuss in §4.

Now let's analyze the energetics of the three models. We define the advection factor of hot accretion flow as the ratio of the energy advection rate to the viscous dissipation rate:

$$f \equiv \frac{Q_{\text{adv}}}{Q_{\text{vis}}} = 1 - \frac{Q_{\text{rad}}^-}{Q_{\text{vis}}}. \quad (7)$$

Here  $Q_{\text{adv}} \equiv \rho \frac{d(e/p)}{dt} + p \nabla \cdot \mathbf{v} \equiv \rho T dS/dt$  ( $S$  is the entropy) is the so-called advection term and  $Q_{\text{vis}} \equiv \mathbf{T}^2/\mu$  is the viscous dissipation rate (ref. eq. 3). Figure 4 shows the time-averaged advection factor near the equatorial plane of the three models. The result is similar if we move away from the equatorial plane. We can see from the figure that  $f$  is almost equal to 1 for Models B and C, i.e., they are fully advection-dominated. This is because the radiative cooling is negligible compared to viscous dissipation. With the increase of accretion rates, radiation becomes more and more

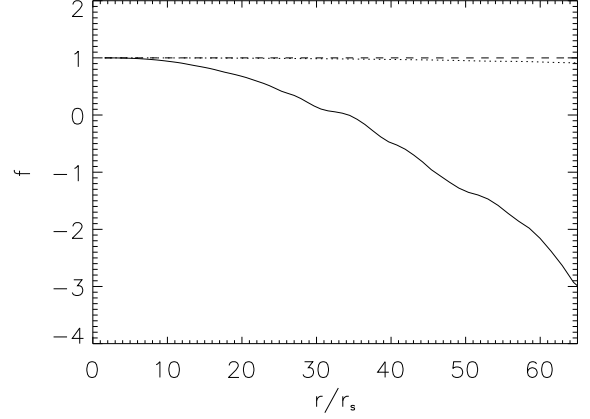


**Figure 4.** Time-averaged advection factor  $f$  (ref. eq. 7) near the equatorial plane. The solution is averaged over angle between  $\theta = 84^\circ$  and  $\theta = 96^\circ$ . The solid, dotted and dashed lines correspond to Model A (LHAF), B (ADAF), and C (ADAF), respectively.

important. The rate of viscous heating

$$\mathbf{T}^2/\mu \propto \mu r^{-3} \propto \rho r^{-3},$$

and the rate of radiative cooling is

$$Q_{\text{rad}}^- \propto \rho^2 T^{1/2} \propto \rho^2 r^{-3/4}.$$

Thus there exists a critical accretion rate  $\dot{M}_{\text{crit}}$ , determined by  $f = 0$ , and we have  $\dot{M}_{\text{crit}} \propto r^{-9/4}$ . Beyond this critical rate, the ADAF solution does not exist since the radiative cooling is stronger than viscous heating thus  $f < 0$  (Abramowicz et al. 1995; Narayan, Mahadevan & Quataert 1998). This is the case for Model A, where we have  $f < 0$  for  $r > 30 r_s$ . But note that the accretion flow still remains hot in this case, as shown in Figure 2. This is because the sum of the viscous dissipation and compression work is still larger than the radiative cooling. In this case, the gradient of entropy of accretion flow, i.e., the left-hand side of the energy equation, is negative, so advection plays a heating role. This type of accretion flow is different from ADAFs; instead, it is called the luminous hot accretion flow (LHAF; Yuan 2001), which is an extension of ADAFs to higher accretion rates.

### 3.2 Convective instability

The condition for convective instability in a rotating accretion flow is:

$$N_{\text{eff}}^2 \equiv N^2 + \kappa^2 = -\frac{1}{\rho} \frac{dP}{dR} \frac{d \ln(P^{1/\gamma}/\rho)}{dR} + \kappa^2 < 0, \quad (8)$$

where  $N$  is the usual Brunt-Väisälä frequency and  $\kappa$  is the epicyclic frequency which is equal to rotation angular velocity  $\Omega$  for nearly Keplerian rotation (Narayan & Yi 1994). For a non-rotating flow,  $\kappa = 0$ , this condition is then equivalent to an inward increase of entropy, which is the well-known Schwarzschild criterion. For a rotating flow, the inward increase of entropy is a necessary condition for convective instability. In other words, the flow must be convectively stable if the entropy decreases inwardly.



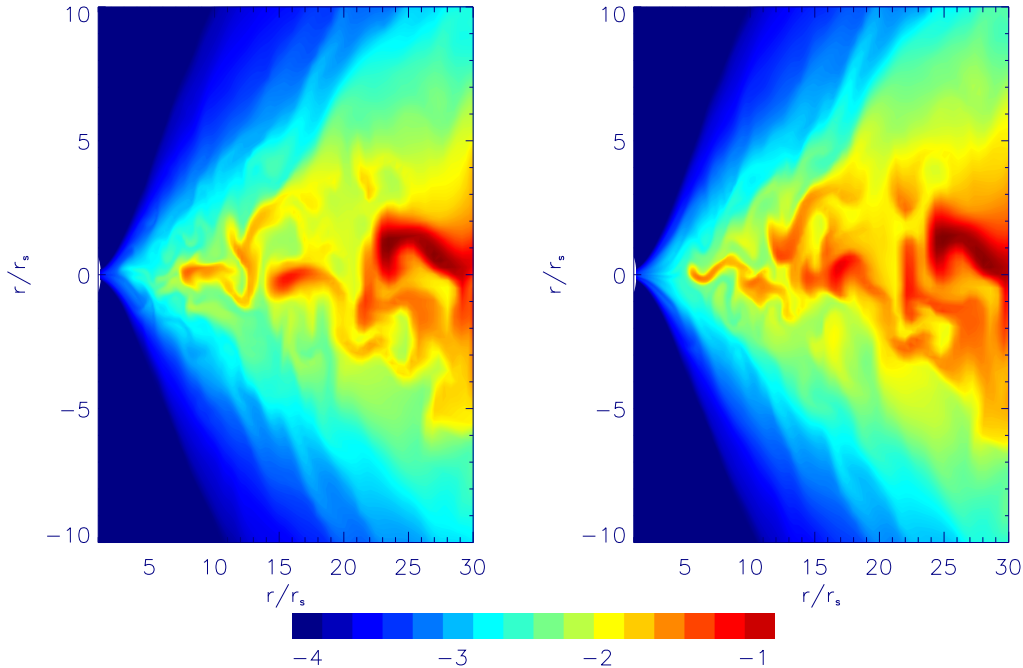


**Figure 5.** Snapshots of the logarithm of the density at  $t=15$  orbits for Model A (left) and B (right).

As we state in introduction, numerical simulations show that an ADAF without radiation is convectively unstable (IA99; SPB99; Igumenshchev & Abramowicz 2000). This is because of the inward increase of entropy in an ADAF (Narayan & Yi 1994). Following SPB99, if we define the mass inflow, outflow, and net rates as,

$$\dot{M}_{\text{in}}(r) = 2\pi r^2 \int_0^\pi \rho \min(v_r, 0) \sin \theta d\theta, \quad (9)$$

$$\dot{M}_{\text{out}}(r) = 2\pi r^2 \int_0^\pi \rho \max(v_r, 0) \sin \theta d\theta, \quad (10)$$

$$\dot{M}_{\text{net}}(r) = \dot{M}_{\text{in}}(r) - \dot{M}_{\text{out}}(r), \quad (11)$$

as a result of convective instability, both the mass inflow and outflow rates decrease inward (ref. Fig. 6 in SPB99). This is physically because of convective outflow (note that these outflow can't escape to infinity because of their negative value of Bernoulli parameter) and gas circulation in convective eddies. This is one of the most important results of previous hydrodynamical simulations of hot accretion flows in the past decade.

All previous studies neglect radiation. In reality, radiation is strong in many, if not most, of black hole systems. A natural question is then whether the flow is the convectively stable or not in this case<sup>1</sup>. When radiation is important, it is possible that the convective instability may become weaker

or even becomes convectively stable. This is because, qualitatively, radiation plays a similar role to convection in terms of carrying away the dissipated energy. Quantitatively, the inclusion of radiation will change the gradient of entropy. The energy equation (eq. 3) can be re-written as:

$$\rho T \left( \frac{\partial S}{\partial t} + \mathbf{v} \cdot \nabla S \right) = \mathbf{T}^2 / \mu - Q_{\text{rad}}^- \quad (12)$$

So the inclusion of radiation will make the radial profile of entropy flatter. If radiation is strong enough so that  $Q_{\text{rad}}^- > Q_{\text{vis}} (\equiv \mathbf{T}^2 / \mu)$ , as in an LHAF, the gradient of entropy will change sign. For a one-dimensional LHAF, this implies

$$\rho T v_r \frac{\partial S}{\partial r} = \mathbf{T}^2 / \mu - Q_{\text{rad}}^- < 0. \quad (13)$$

This means that the entropy of an LHAF will decrease inwardly ( $v_r < 0$ ). Therefore, Yuan (2001) speculates that different from an ADAF, an LHAF should be convectively stable.

However, our two-dimensional numerical simulations indicate that this is not true. We find that Model A is also convectively unstable. The two plots in Figure 5 show the snapshots of the logarithm of the density at  $t = 15$  orbits for Models A (left plot) and B (right plot), respectively. It is hard to tell any significant difference between them. In both plots the large-amplitude fluctuations at small scales which is associated with convective motion are evident. We calculate the Brunt-Väisälä frequency  $N_{\text{eff}}$  (eq. 8) and do find  $N_{\text{eff}}^2 < 0$  in most of the region of the accretion flow for both Model A and B, as shown by Figure 6.

We also calculate the mass fluxes of the three models based on eqs. (9-11). The results are shown in Figure 7.

<sup>1</sup> We neglect the thermal instability in our discussion, because even though an LHAF is thermally unstable, the growth timescale of perturbation is longer than the accretion timescale (Yuan 2003).

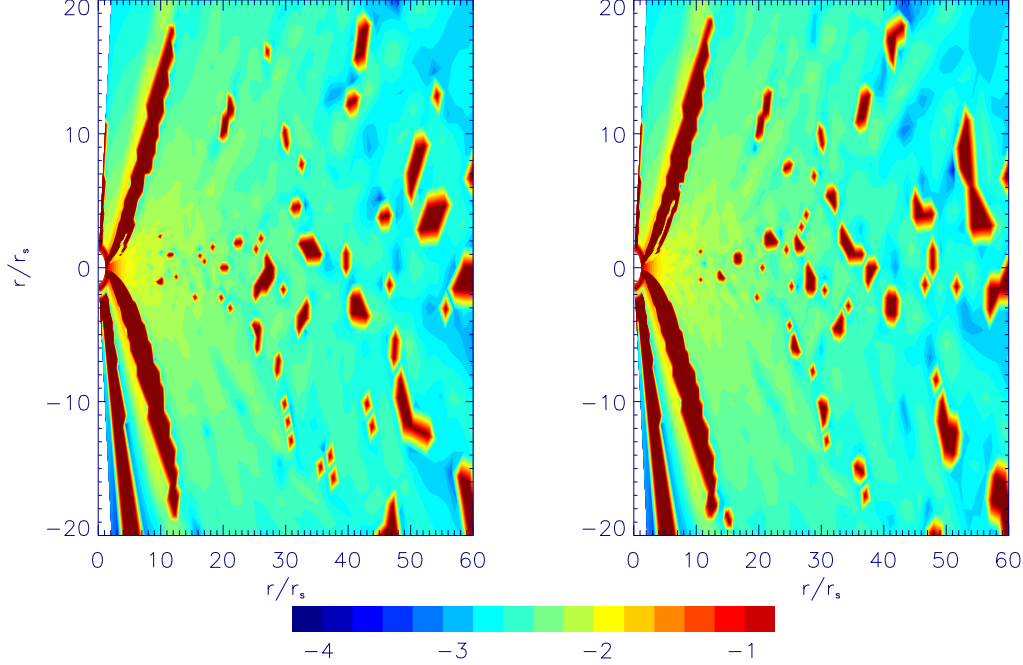


**Figure 6.** Snapshots of  $N_{\text{eff}}^2$  at  $t=15$  orbits for Model A (left) and B (right). The red region denotes  $N_{\text{eff}} > 0$ , all other colors denote  $N_{\text{eff}} < 0$ . We can see that for both models,  $N_{\text{eff}}^2 < 0$  in most of the region. The labels of the color bar is the logarithm of the absolute value of  $N_{\text{eff}}$ .

The black, red, and blue lines correspond to Model A, B, and C, respectively. In each model, the solid, dashed, and dotted lines denote the rates of inflow, outflow, and net accretion, respectively. In all cases, the net accretion rate is constant with radius, which indicates that our simulations have achieved quasi-steady state. In all three models, the inflow rate  $\dot{M}_{\text{in}}$  and outflow rate  $\dot{M}_{\text{out}}$  decrease inward because of the convective instability, as we expect, with almost the same “steepness”. Quantitatively, the net accretion rates of Models A, B, and C are  $\dot{M}_{\text{net}} = \dot{M}_{\text{in}}(r) - \dot{M}_{\text{out}}(r) = 6.4 \times 10^{-4}$ ,  $3.97 \times 10^{-6}$  and  $4.02 \times 10^{-8} \dot{M}_{\text{Edd}}$ , respectively. If the radiation does not affect the strength of convection, we would expect that the net accretion rates differ by exactly 100 times from Model A to B, and B to C, respectively. So such a result indicates that radiative cooling does weaken the convective instability. Correspondingly we find that the ratio of the energy flux associated with convection and with advection is moderately weaker in Model A than those of Model B and C. But we want to emphasize that such an effect is very weak.

The result that Model A is also convectively unstable is in conflict with the one-dimensional prediction. To examine the reason of convective instability of Model A, in Figure 8 we show the radial and angular structures of entropy ( $S = \ln P - \gamma/(\gamma-1) \ln T$ ) of the three models. The radial structure along the equatorial plane is shown in the upper panel (the result along  $\theta = 45^\circ$  is similar). The middle and lower panels show the angular structure at  $r = 20$  and  $40 r_s$ , respectively. The entropy increase inward in most of the region of Model B and C, as we expect. But surprisingly we find that this is

also the case of Model A for  $r < 110 r_s$ , although  $f < 0$  for  $r > 30 r_s$  (ref. Figure 4). *It is the increase of entropy along the equatorial plane (the direction of the gravitational force) that results in the convective instability of Model A.*

The inward increase of entropy in Model A is not in contradiction with the negative value of advection factor  $f$ . For a steady two-dimensional LHAF, the energy equation (12) reduces to,

$$\rho T \mathbf{v} \cdot \nabla S \equiv \rho T \left( v_r \frac{\partial S}{\partial r} + v_\theta \frac{\partial S}{\partial \theta} \right) = Q_{\text{vis}} - Q_{\text{rad}}^- < 0. \quad (14)$$

From Figure 8 we see that  $\partial S / \partial r < 0$ ,  $\partial S / \partial \theta < 0$  (for  $\theta < \pi/2$ ) and  $\partial S / \partial \theta > 0$  (for  $\pi > \theta > \pi/2$ ). Eq. (14) is satisfied because we have  $v_r < 0$  and  $v_\theta > 0$  (for  $\theta < \pi/2$ ) and  $v_\theta < 0$  (for  $\pi > \theta > \pi/2$ ). If without the  $v_\theta (\partial S / \partial \theta)$  term, i.e., for the one-dimensional case, from  $f < 0$  we would have  $\partial S / \partial r > 0$ , i.e., the flow is convectively stable.

### 3.3 Varying the form and amplitude of shear stress

All the simulations described so far are based on the viscosity stress description of  $\nu \propto \rho$ . In this case,  $\rho(r) \propto r^0$  (SPB99). We have also tried the description of  $\nu \propto r^{1/2}$  which is the usual “ $\alpha$ ” description. This is the description adopted in IA99 and Run K in SPB99. Under this description, the density profile is steeper,  $\rho \propto r^{-1/2}$  (SPB99). The higher density at the innermost region makes the bremsstrahlung radiation much stronger compared to the former description. From eq. (14) we see that  $\mathbf{v} \cdot \nabla S$  will

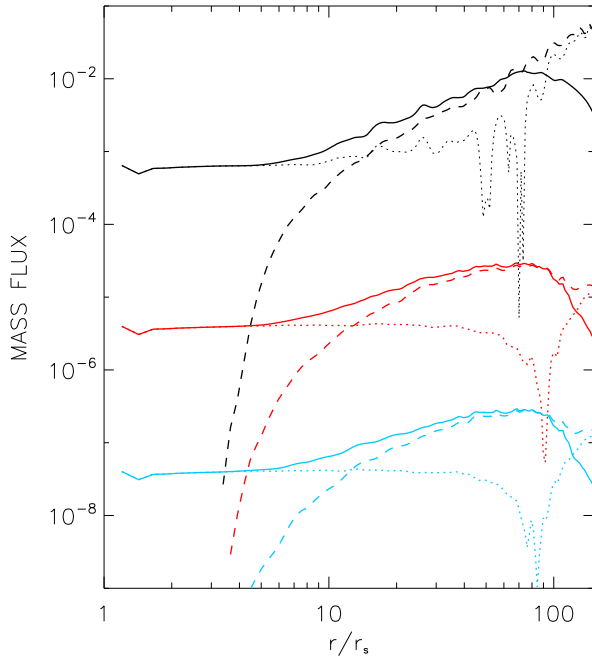


**Figure 7.** Time-averaged mass fluxes measured in units of Edington accretion rate. The black, red, and blue lines correspond to Model A, B, and C, respectively. In every model, the solid, dotted and dashed lines denote the inflow rate, net accretion rate and outflow rate, respectively.

become “more negative”. We therefore need to check the convective instability in this case.

For this aim, we simulate three models with this kind of viscous stress description. All other parameters are the same as Model A, B, and C<sup>2</sup>. Specifically, for Model A which has the highest accretion rate, the advection factor  $f < 0$  for  $r > 40r_s$ . Our simulation results indicate that all three models are again convectively unstable, with  $N_{\text{eff}}^2 < 0$  in most of the region, as in the cases presented in §3.2. Because of the convective instability, the mass fluxes again decrease inward, as shown by Fig. 9. The physical reason is same to the cases of the former viscous stress description. Figure 10 shows the radial and angular profiles of entropy. We see from the figure that the flow adjusts itself so that the entropy increases radially inward, although the advection factor  $f < 0$ .

IA99 find that when the viscous stress is large,  $\alpha \sim 1$  in the language of the  $\alpha$  description ( $\nu \propto r^{1/2}$ ), the convective instability disappears and the accretion flow shows powerful unbound bipolar outflow structure. SPB99 also simulated the case of large viscous stress. Different from IA99, they find that convective instability still exists. They speculate that the discrepancy may be because that the poloidal components of the shear stress tensor adopted in IA99 suppress

<sup>2</sup> Because of the difference of the viscous stress description, the accretion rates of each three models here are  $\sim 3$  times smaller compared to those in §3.1, although the density of the initial torus is the same.

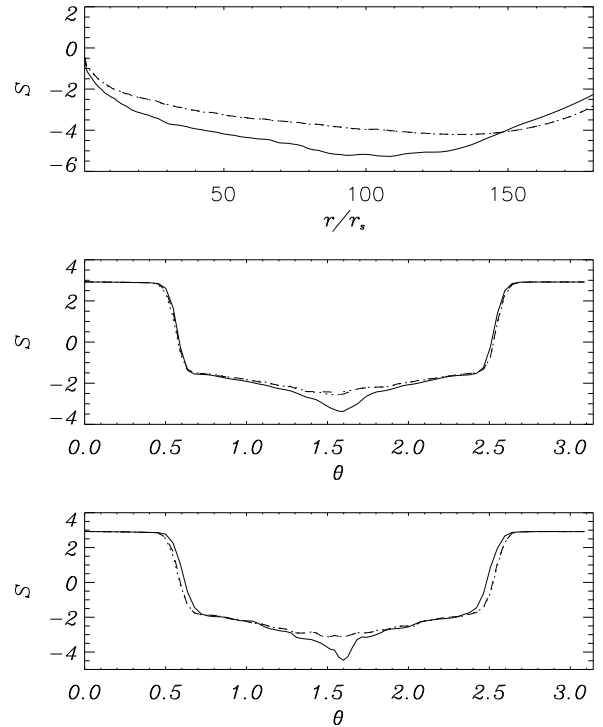


**Figure 8.** The radial (upper panel) and angular (lower two panels) structure of the specific entropy of Models A, B and C. The middle and lower panels show the angular structure at  $r = 20$  and  $40r_s$ , respectively. The solid, dotted, and dashed lines show Model A, B, and C, respectively. For the radial structure, the solution is averaged over angle between  $\theta = 84^\circ$  and  $\theta = 96^\circ$ .

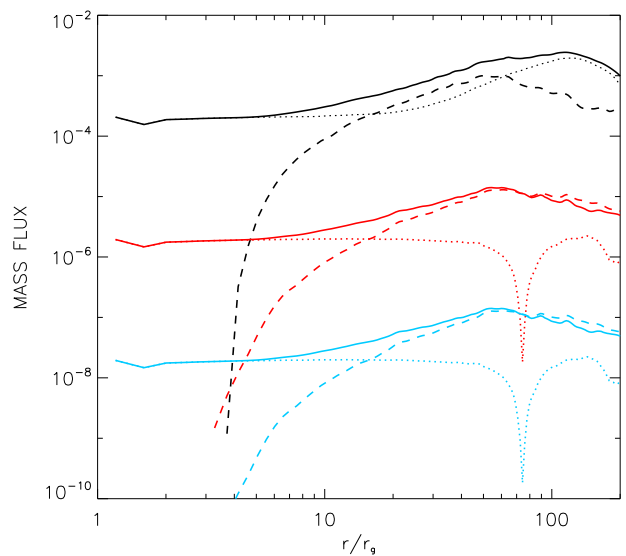


**Figure 9.** Time-averaged mass fluxes measured in units of Edington accretion rate for viscosity stress description  $\nu \propto r^{1/2}$ . The black, red, and blue lines correspond to Model A, B, and C, respectively. In every model, the solid, dotted and dashed lines denote the inflow rate, net accretion rate and outflow rate, respectively.



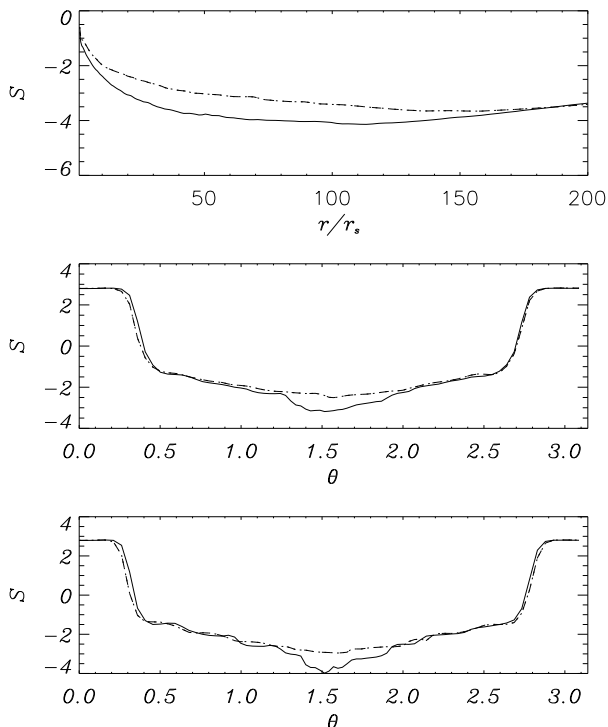


**Figure 10.** The radial (upper panel) and angular (lower two panels) structure of the specific entropy of Models A, B and C for the  $\nu \propto r^{1/2}$  viscosity stress description. The middle and lower panels show the angular structure at  $r = 20$  and  $40r_s$ , respectively. The solid, dotted, and dashed lines show Model A, B, and C, respectively. For the radial structure, the solution is averaged over angle between  $\theta = 84^\circ$  and  $\theta = 96^\circ$ .

the convection. But the simulation of SPB99 is based on the  $\nu \propto \rho$  description which is different from IA99. Although this is not expected to bring significant difference on the existence of convective instability, it is more direct to adopt the  $\nu \propto r^{1/2}$  stress description to check the result. We adopt such a viscous description and find that in the case of a large  $\alpha$ , when all the components of the shear stress are adopted, we do recover the results of IA99, namely convective instability dies off and the accretion flow shows bipolar outflow structure. However, when only the azimuthal components are adopted as in SPB99, we find that the accretion flow is still convectively unstable even though  $\alpha$  is large.

#### 4 SUMMARY AND DISCUSSION

Previous works without including radiation indicate that the flow is strongly convectively unstable. We have investigated the effects of radiation on the properties of hot accretion flows based on two-dimensional hydrodynamical numerical simulations. Special attention is paid to the convective instability of accretion flow when radiative cooling is strong. This question is important since it determines the radial profile of accretion rate and thus the observational appearances of black hole system, and the evolution of black hole mass and spin.

We consider the effects of radiation by including a

bremssstrahlung radiation term in the energy equation. Three models (Model A, B, and C) are adopted with mass accretion rates spanning four orders of magnitude. We find that with the increase of accretion rate, the flow becomes cooler thus the mass more concentrated onto the equatorial plane. In all cases, the Bernoulli parameter is always negative, except in the small region close to the poles. This results in very weak unbound outflow, with the mass flux being only 1% of the inflow rate.

Radiation is very weak in Model B and C thus they are convectively unstable. For the model with the highest accretion rate (Model A), the radiative cooling is so strong that it is larger than the viscous heating in most of the region, i.e., the advection factor is negative (ref. Figure 4). This model thus belongs to the regime of luminous hot accretion flow (LHAF; Yuan 2001). LHAF is speculated to be convectively stable in the one-dimensional analysis because the entropy decreases inward (Yuan 2001). However, our simulations indicate that such a one-dimensional result is not correct. Same with Model B and C, Model A is also convectively unstable (Figures 5&6). As a result, the inflow and outflow rates are decreasing inward, with almost the same “steepness” of the profile of mass flux for all three models (Figure 7). We find that the reason is because the entropy increases radially inward in two-dimensional case (Figure 8).

We only consider bremssstrahlung radiation in our work. As a result, the advection factor is always positive in the most interesting innermost region, even though a large accretion rate is adopted. It will be interesting to investigate the convective instability of a model with a negative  $f$  in the whole region of the accretion flow. This can be achieved in principle by adopting a higher accretion rate. But the problem is that if a much larger accretion rate were adopted, the radiation at the outer region will become so strong that the hot accretion flow will collapse. One way to avoid this problem is to include synchrotron radiation and especially its Comptonization. Since they are much stronger than the bremssstrahlung radiation at the innermost region of the flow, the advection factor at small radii will easily become negative, even smaller than that in the outer region (ref. Yuan 2001). The convective stability in this case will be an important project.

In this paper we consider the effects of radiation only by including a radiative cooling term in the energy equation. Further improvement on radiation can be done by calculating the radiative transfer. For hot accretion flows, the radiation pressure is always smaller than the gas pressure thus the effect of radiation in the momentum equation can be neglected. But the interaction of energy between radiation and gas will be important when the accretion rate is large. Since the radial optical depth of accretion flow is less than unity, the radiation produced at one radius can propagate for a large distance and heat or cool gas at other radius via Compton scattering. As a result, the dynamics of the accretion flow will be significantly changed (e.g., Ostriker et al. 1976; Cowie et al. 1978; Park & Ostriker 1999; 2001; 2007; Yuan, Xie & Ostriker 2009; Xie et al. 2010). At the outer region, such Compton scattering plays a heating role. It is found that the self-consistent solution including this effect can only exist below a certain accretion rate, because the flow beyond a certain large radius will be heated above the

virial temperature thus the accretion is suppressed<sup>3</sup>. Above this value, the black hole will oscillate between an active and inactive phase (Cowie et al. 1978; Yuan, Xie & Ostriker 2009). Time-dependent numerical simulation is required to check these analytical results. Regarding the convective instability, Compton scattering will heat gas at large radii but cool gas at inner region, thus the entropy of the flow will become larger at outer region but smaller at inner region. So the entropy will decrease faster inward compared to Model A in the present paper. Whether this is sufficient to change the sign of the gradient of entropy and thus stabilize the accretion flow against the convective instability is another interesting project.

We adopt an anomalous shear stress to transfer the angular momentum. In reality, magnetic field must exist and the turbulence associated with the magnetorotational instability (MRI) is believed to be the origin of viscosity. A question is then whether the hydrodynamical analysis adopted in the present paper is applicable to a magneto-hydrodynamical (MHD) flow. There have been some discussions in the literature on this point (Hawley, Balbus, & Stone 2001; Balbus & Hawley 2002; Narayan et al. 2002). Narayan et al. (2002) show that if the magnetic field saturates at a value sufficiently below equipartition, convective fluctuations can be applicable to an MHD accretion flow (since long-wavelength convective fluctuations can fit inside the accretion disk). Unfortunately, the saturated magnetic field in MRI simulation of accretion flow seems to be not universal, e.g., depending on the initial configuration of the magnetic field (Stone & Pringle 2001; Machida et al. 2001). Although our focus of the present work is on the main body of accretion flow, we would like to mention in this context that the coronal region of accretion flow is known to be strongly magnetized, with magnetic field there exceeding the equipartition strength (e.g., Miller & Stone 2000; Beckwith, Hawley & Krolik 2008). So our hydrodynamical analysis does not apply in that region.

We mention in the introduction that the luminosity of black hole X-ray binary almost remains constant before and after the state transition. If the hot accretion flow is still convectively unstable after all the above-mentioned effects have been taken into account, which implies that the accretion rate decreases inward from the transition radius  $R_{tr}$ , the value of  $R_{tr}$  must be small so that the accretion rates of the inner hot and outer cool accretion flows are similar. This puts an independent constraint on the mechanism of transition from an outer cold disk to an inner hot accretion flow.

## 5 ACKNOWLEDGMENTS

We thank Woong-Tae Kim and Ramesh Narayan on their valuable comments on the paper. We also benefit signifi-

cantly from the advices of Woong-Tae Kim on the ZEUS code. The idea of considering radiative cooling is stimulated from the discussion with James Stone. We also thank the referee for his/her constructive suggestions which greatly improve the presentation of the paper. This work was supported in part by the Natural Science Foundation of China (grants 10773024, 10833002, 10821302, and 10825314), the National Basic Research Program of China (973 Program 2009CB824800), and the CAS/SAFEA International Partnership Program for Creative Research Teams.

## REFERENCES

- Abramowicz M. A., Chen X., Kato S., Lasota J.-P., Regev O., 1995, *ApJ*, 438, L37
- Baganoff F. K., Maeda Y., Morris M., Bautz M. W., Brandt W. N., Cui W., Doty J. P., Feigelson E. D., Garmire G. P., Pravdo S. H. and 2 coauthors, 2003, *ApJ*, 591, 891
- Balbus S. A., Hawley J. F., 1998, *Rev. Mod. Phys.*, 70, 1
- Balbus S. A., Hawley J. F., 2002, *ApJ*, 573, 749
- Beckwith, K., Hawley, J. F. & Krolik, J. H. 2008, *ApJ*, 678, 1180
- Blandford R. D., Begelman M. C., 1999, *MNRAS*, 301, L1
- Cowie L. L., Ostriker J. P., Stark A. A., 1978, *ApJ*, 226, 1041
- Hayes J. C., Norman M. L., Fiedler R. A., Borden J. O., Li P. S., 2006, *ApJ*, 165, 188
- Hawley, J. F., Balbus, S. A., & Stone, J. M. 2001, *ApJ*, 554, L49
- Ho L., 2008, *ARA&A*, 46, 475
- Igumenshchev I. V., Abramowicz M. A., 1999, *MNRAS*, 303, 309
- Igumenshchev I. V., Abramowicz M. A., 2000, *ApJS*, 130, 463
- Johnson, B. M. & Quataert, E. 2007, *ApJ*, 660, 1273
- Machida M., Matsumoto R., Mineshige S., 2001, *PASJ*, 53, L1
- Marrone D. P., Moran J. M., Zhao J. H., Rao R., 2007, *ApJ*, 654, L57
- McKinney J. C., Gammie C. F., 2002, *ApJ*, 573, 728
- Miller, K. A., & Stone, J. M. 2000, *ApJ*, 534, 398
- Narayan R., 2005, *Ap&SS*, 300, 177
- Narayan R., Igumenshchev I. V., Abramowicz M. A., 2000, *ApJ*, 539, 798
- Narayan R., McClintock J.E., 2008, *New Astron. Rev.*, 51, 733
- Narayan R., Quataert E., Igumenshchev I. V., Abramowicz M. A., 2002, *ApJ*, 577, 295
- Narayan R., Yi I., 1994, *ApJ*, 428, L13
- Narayan R., Yi I., 1995, *ApJ*, 452, 710
- Narayan R., Mahadevan R., Quataert E., 1998, in Abramowicz M. A., Björnsson G., Pringle J. E., eds, *Theory of Black Hole Accretion Discs*. Cambridge Univ. Press, Cambridge, p. 148
- Ostriker J. P., McCray R., Weaver R., Yahil A., 1976, *ApJ*, 208, L61
- Papaloizou J. C. B., Pringle J. E., 1984 *MNRAS*, 208, 721
- Park M., Ostriker J. P., 1999, *ApJ*, 527, 247
- Park M., Ostriker J. P., 2001, *ApJ*, 549, 100
- Park M., Ostriker J. P., 2007, *ApJ*, 655, 88
- Quataert E., Gruzinov A., 2000, *ApJ*, 539, 809
- Stone J. M., Pringle J. E., Begelman M. C., 1999, *MNRAS*, 310, 1002
- Stone J. M., Pringle J. E., 2001, *MNRAS*, 322, 461
- Tanaka, T., & Menou, K. 2006, *ApJ*, 649, 345
- Xie F.G., Niedzwiecki A., Zdziarski A. A., Yuan F., 2010, *MNRAS*, 403, 170X
- Yuan F., 2001, *MNRAS*, 324, 119
- Yuan F., 2003, *ApJ*, 594, L99
- Yuan F., Xie F.G., Ostriker J. P., 2009, *ApJ*, 691, 98
- Yuan F., 2007, in Luis C. Ho., Jian-Min Wang, eds, *ASP conf. Ser.*, Vol. 373, *The Central Engine of Active Galactic Nuclei*. Astron. Soc. Pac., San Francisco, p. 95
- Zdziarski A. A., Gierlinski M., Mikoajewska J., Wardzinski G.,

<sup>3</sup> Any significant energy flux from the inner to the outer region of an accretion flow can reduce the mass inflow rate. In addition to convection which is the focus of this paper, radiation is another mechanism of transferring energy outward (Ostriker et al. 1976). Other examples include viscous stresses (Blandford & Begelman 1999) and thermal conduction (Tanaka & Menou 2006; Johnson & Quataert 2007).

Smith D. M., Harmon B. A., Kitamoto S., 2004, MNRAS,  
351, 791